Research Square

Preprints are preliminary reports that have not undergone peer review.
They should not be considered conclusive, used to inform clinical practice,
or referenced by the media as validated information.

Supernatant from primary human gut microbiota fermentation as a modulator of intestinal barrier in in vitro models

Sofia Sousa
International Iberian Nanotechnology Laboratory
Patrícia Rodrigues
International Iberian Nanotechnology Laboratory
Verônica Morato
International Iberian Nanotechnology Laboratory
Mafalda Neto
International Iberian Nanotechnology Laboratory
Enriqueta Garcia-Gutierrez
Teagasc Food Research Centre
Victor Calero
International Iberian Nanotechnology Laboratory
Paul Cotter
Teagasc Food Research Centre
Lorenzo Pastrana
International Iberian Nanotechnology Laboratory
Catarina Gonçalves
catarina.goncalves@inl.int

International Iberian Nanotechnology Laboratory

Article

Keywords: differentiated Caco-2/HT29-MTX cultures, transepithelial electrical resistance, lucifer yellow permeability, inflammation, cell culture inserts, gut-chip

Posted Date: November 3rd, 2026

DOI: https://doi.org/10.21203/rs.3.rs-11220874/v1

License: This work is licensed under a Creative Commons Attribution 4.0 International License.
Read Full License

Additional Declarations: No competing interests reported.

Abstract

The human intestine harbours a complex microbial community that closely interacts with intestinal epithelial cells, the first line of host defence. Although several *in vitro* models have been developed to study host–microbiota interactions, direct co-culture of gut microbiota and mammalian cells remains technically challenging. Here, we evaluated an in vitro approach for testing human faecal fermentation supernatant on intestinal barrier function using differentiated Caco-2/HT29-MTX monolayers maintained in static cell culture inserts or a dynamic gut-chip model. Fermentation supernatant diluted in HBSS was applied for 4 h, and barrier function was assessed by transepithelial electrical resistance (TEER) in static cultures and by Lucifer Yellow apparent permeability (P_{app}) in both models. Under the conditions tested, exposure to the fermentation supernatant did not compromise barrier integrity. Lucifer Yellow Papp was significantly lower in cell culture inserts ($1.04\times10^{-7}\pm8.98\times10^{-9}$ cm·s^{-1}) than in the dynamic gut-chip ($7.96\times10^{-7}\pm1.82\times10^{-7}$ cm·s^{-1}), highlighting differences in epithelial permeability between static and dynamic culture conditions. To enable prolonged exposure studies, different carrier conditions were evaluated. HBSS was unsuitable for 24 h incubation, resulting in reduced cell metabolic activity and TEER, whereas HBSS-HEPES maintained cell viability and barrier function. A TNF-α-induced barrier dysfunction was subsequently established, resulting in a 45% decrease in TEER and a 48% increase in Lucifer Yellow P_{app} compared with the healthy control. Treatment with fermentation supernatant diluted in HBSS-HEPES was associated with a reduction in the increased permeability, with P_{app} values becoming comparable to those of the healthy control condition. restored barrier integrity, demonstrating its capacity to repair impaired intestinal epithelial. Overall, this study establishes a practical *in vitro* framework for evaluating faecal fermentation-derived products using intestinal epithelial models representing both healthy and barrier-impaired conditions. The findings highlight the importance of selecting appropriate culture platforms, carrier conditions, and exposure periods when assessing the effects of complex microbiota-derived products on intestinal barrier function and provide a basis for the subsequent testing of fermentation samples in cell-based intestinal models.

1. Introduction

The intestinal barrier is a complex physiological system that regulates interactions between the host and its environment and is essential for maintaining intestinal homeostasis. Its physical barrier function relies primarily on the structural and functional integrity of the intestinal epithelium, which is supported by intercellular tight junction (TJ) complexes and a protective mucus layer overlying the epithelial surface [1]. Under inflammatory conditions, disruption of epithelial TJ compromises the barrier function, increasing intestinal permeability. However, the relationship between barrier dysfunction and inflammation is complex, and it remains unclear whether increased intestinal permeability is a cause or a consequence of the inflammatory response [2, 3]. The human gut microbiota is a complex and dynamic ecosystem whose composition and diversity are shaped by multiple factors, including dietary habits, lifestyle, genetic background, and environmental conditions [4]. Among its many functions, the gut microbiota contributes to the fermentation of dietary fibres, generating a range of metabolites, including

short-chain fatty acids (SCFAs), such as acetate, propionate, and butyrate [5]. These metabolites are involved in multiple physiological processes, including intestinal epithelial metabolism, immune modulation, and maintenance of intestinal homeostasis [6, 7]. SCFAs have also been associated with the maintenance of intestinal barrier function through mechanisms involving mucus production and regulation of TJ proteins[8–10]. However, the effects of SCFAs and other microbiota-derived metabolites on the intestinal epithelium are dependent on their concentration, composition, and local environmental conditions. Consequently, exposure to elevated concentrations or altered metabolite profiles may adversely affect epithelial cells and barrier function [11, 12]. Given the complexity of the gut microbial metabolome, approaches that enable the evaluation of the combined effects of microbiota-derived products on intestinal epithelial function are therefore of particular interest.

The development of reliable *in vitro* intestinal models has become increasingly important for investigating intestinal physiology, barrier dysfunction, and inflammation, particularly in the context of the development and application of non-animal methods [13, 14]. Reproducing relevant features of the human intestinal epithelium and microbiota-derived components *in vitro* provides an opportunity to investigate mechanisms associated with barrier dysfunction and to evaluate potential interventions under controlled experimental conditions. Consequently, alternative *in vitro* models are being developed to reproduce key structural and functional characteristics of the human intestine and to improve the physiological relevance of experimental studies [3]. Among cell-based intestinal models, Caco-2 cells are the gold standard for *in vitro* models due to their capacity to undergo spontaneous differentiation into enterocyte-like cells, which represent the predominant epithelial cell type in the small intestine [15, 16]. Caco-2 cells are frequently co-cultured with HT29-MTX cells to introduce a mucus-producing phenotype resembling intestinal goblet cells [17]. The presence of mucus-secreting cells provides a more representative epithelial interface and enables investigation of the influence of the mucus layer on epithelial transport and barrier function [16]. Intestinal epithelial barrier function can be evaluated using complementary approaches, including transepithelial electrical resistance (TEER), determination of the apparent permeability (P_{app}) using marker molecules, and assessment of TJ protein or gene expression by immunostaining and quantitative polymerase chain reaction (qPCR), respectively. Cell-based models using established cell lines offer important advantages in terms robustness, accessibility, simplicity and reproducibility [18].

Conventional two-dimensional (2D) intestinal models are commonly established on cell culture inserts containing semi-permeable membranes, thereby allowing the formation of distinct apical and basolateral compartments. However, do not fully reproduce the complex three-dimensional (3D) architecture and dynamic physical environment of the intestinal epithelium. In particular, epithelial cells cultured under static conditions may exhibit morphological and functional characteristics that differ from those observed *in vivo* [17, 18]. More advanced models, including organoids and gut-chip systems, have therefore emerged as promising platforms for improving the physiological relevance of *in vitro* intestinal studies [19, 20]. These models can reproduce aspects of intestinal 3D architecture, cellular differentiation, and, in the case of dynamic gut-chip systems, controlled fluid flow and other features of the intestinal microenvironment.

Despite these advances, direct co-culture of gut microbiota with mammalian intestinal cells remains technically challenging. Bacterial overgrowth during prolonged culture and the conflicting oxygen requirements of microorganisms and intestinal epithelial cells can compromise the maintenance of both components under suitable experimental conditions [3]. An alternative strategy is to use faecal inocula for in vitro fermentation and generation of fermentation supernatants to subsequently expose intestinal epithelial cells to these complex mixtures of microbiota-derived products. This approach enables the effects of fermentation-derived products on mammalian intestinal cells to be investigated while avoiding some of the challenges associated with maintaining a direct host–microbiota co-culture [21]. Furthermore, the establishment of intestinal barrier dysfunction *in vitro* remains variable across experimental systems, particularly with respect to the inflammatory stimuli employed, their concentrations and exposure periods, culture conditions, and endpoints used to characterise barrier responses[3]. Tumour necrosis factor-α (TNF-α), a key pro-inflammatory cytokine, is frequently used to induce epithelial barrier dysfunction *in vitro* and provides a controlled approach for investigating changes in epithelial permeability and barrier-associated responses. The combination of healthy and experimentally compromised epithelial models can therefore provide complementary information on whether microbiota-derived products are compatible with an intact epithelial barrier and whether they can influence barrier function under conditions of pre-existing dysfunction.

In the present study, we explored the suitability of using human faecal fermentation supernatant to investigate its effects on the intestinal epithelial barrier under both healthy and compromised conditions. Differentiated Caco-2/HT29-MTX (9:1) cultures were established in conventional static cell culture inserts and in a dynamic gut-chip model, providing complementary platforms for evaluating epithelial responses. The effects of the fermentation supernatant on the healthy epithelial barrier were evaluated using cell viability, transepithelial electrical resistance (TEER), lucifer yellow apparent permeability (P_{app}), and TJ protein expression, as appropriate to each experimental model. Different exposure conditions and carriers were also investigated to identify suitable conditions for maintaining epithelial viability and barrier function during prolonged incubation. Finally, a TNF-α-induced barrier dysfunction model was followed to assess whether the fermentation supernatant could modulate a compromised intestinal epithelial barrier. Overall, this study evaluates an *in vitro* approach for testing faecal fermentation supernatants on intestinal epithelial models representing both healthy and barrier-impaired conditions, while examining how the culture platform and experimental conditions influence the assessment of epithelial barrier responses.

2. Materials and methods

2.1. Fermentation from primary human gut microbiota and characterisation

2.1.1. In vitro fermentation

Faecal slurry preparation was conducted as previously described [22]. Ethical approval for the study was granted by the Clinical Research Ethics Committee of the Cork Teaching Hospitals, UCC (ECM 4 (mm) 09/03/2021). Written informed consent was obtained from healthy donors who had not received antibiotic treatment within the preceding six months, after which faecal samples were collected. All methods were carried out in accordance with relevant guidelines and regulations. A total of 200 g of faecal material was maintained at 4°C for 1–2 h, before processing. Faecal sample was processed in an anaerobic chamber containing 5 % C_2, 10 % H, and 85 % N, mixing it with 200 mL of saline buffer supplemented with 0.05 % (/v) cysteine hydrochloride in a Circulator 400 stomacher bag (Seward, UK) and homogenised. The homogenate was then centrifuged at 4000 × g for 25 min, and the resulting pellet was resuspended in PBS, adding sterile glycerol to a final concentration of 25 % (/v), after which 1 mL aliquots were stored at − 80°C. For *in vitro* fermentation, a faecal slurry aliquot was defrosted and diluted 1:10 in faecal fermentation medium [23]. The faecal fermentation was conducted in duplicate for 24 h at 37°C with shaking at 300 rpm, under anaerobic conditions, with no pH control (Applikon Biotechnology). 1 mL aliquots were collected after the fermentation and stored at − 80°C for subsequent analyses.

2.1.2. Characterisation

2.1.2.1 DNA extraction and quantification

The 1 mL aliquots from fermentation had their gDNA extracted using QIAmp PowerFecal ProDNA kit (Qiagen, Crawley, UK), following manufacturer's instructions. Briefly, samples were centrifuged (4000 x g, 10 min) and resuspended in lysis buffer and the extractions were performed according to the manufacturer's instructions. DNA was quantified using the Qubit 2.0 Fluorometer (Life Technologies, USA) and the purity checked using the NanoDrop 1000 (ThermoFisher Scientific, Ireland).

2.1.2.2 Sequencing and bioinformatics analyses

DNA was prepared according to the Nextera XT DNA library preparation guide from Illumina and sequenced on an Illumina NextSeq Platform (Teagasc, Moorepark Sequencing Facility) using 2 x 150 bp paired-end kit. Raw sequencing data was processed using Shaman to obtain frequency and taxonomy tables [24]. Further processing was conducted using the Qiime2 tools in the Galaxy platform (Galaxy Version 2025.10.0 + q2galaxy.2025.10.0) and visualised in Qiime2 (v 2025.10.0) following standard workflows [25].

2.1.2.3 Organic acid quantification

Defrosted 1 mL aliquots from fermentation underwent filter sterilisation using 0.2 µm-pore-size syringe filters (Whatman International Ltd, UK), and 300 µL of the resulting solution was injected into Chromacol vials (Fisher Scientific, UK). The concentrations of formic, acetic, lactic, citric, propionic, and butyric acid were quantified through High-Performance Liquid Chromatography (HPLC) employing a Perkin-Elmer Flexar HPLC system. Refractive index and photo diode array detectors were used for 210, 280, and 325 nm wavelengths (PerkinElmer Inc, USA). Analyses were conducted using a RezexTM ROA-Organic Acid H+ (8%) LC column coupled with a refractive index detector set at a sensitivity of 512. The column

temperature was maintained at 60°C, and the eluent 0.005 N H2SO4 ran at 0.6 mL·min−1. A standard curve ranging from 10 µg·mL−1 to 100 µg·mL−1 for formic, acetic, lactic, citric, propionic, and butyric acids (all from Sigma-Aldrich) was employed for concentration determination.

2.2. Microfluidic device: Gut-chip

2.2.1. Design and fabrication

The gut-chips fabricated from polydimethylsiloxane (PDMS) consisted of two parallel microchannels separated by a porous PDMS membrane. The channel´s surface area is 19.5 mm², with a total length of 19.5 mm and a width of 1 mm; the culture region spanned 10 mm in length. The semi-permeable PDMS membrane was fabricated using silicon wafer master moulds featuring micropillar arrays with a pyramidal shape (8 µm top diameter top, 12 µm bottom diameter, 40 µm pitch, and 50 µm height). PDMS replicas of the top and bottom layers of the device were produced by casting PDMS on a polymethyl methacrylate mould. The device components were properly bonded using O_2 plasma treatment, as shown in Supplementary Material, Figure S1A.

2.2.2. PDMS membrane functionalization and coating with extracellular matrix (ECM)

After device fabrication, the gut-chips were sterilised by incubation in 70% (v/v) ethanol for 30 min and then rinsed with PBS. To activate the PDMS surface, 0.5 µg•mL^{-1} of sulfo-SANPAH (Thermo Fisher Scientific, Waltham, MA, USA) in sterile distilled water (di$H_2$0) was introduced into the top channel and exposed to UV light (365 nm, 6.8 W, 5 cm distance) for 30 min. The solution was then removed, and the channel was washed with sterile di$H_2$0. After sulfo-SANPAH activation, an ECM coating solution consisting of 30 µg·mL^{-1} collagen type-I (Gibco, Thermo Fisher, MA, USA) and 100 µg·mL^{-1} Matrigel (Corning, MA, EUA) diluted in serum-free high glucose Dulbecco's modified Eagle's medium (DMEM) (PAN-Biotech, GmbH, Aidenbach, Germany) was added to the top channel. The device was incubated overnight at 4°C. An additional 1 h incubation was performed, the next day, at 37°C. Following incubation, both channels were washed with warmed serum-free DMEM to remove non-cross-linked proteins.

2.3. Cell cultures

Caco-2 cells (clone HTB-37, American Type Culture Collection, passages 29–50) were maintained in Minimum Essential Media (MEM), supplemented with 20% (v/v) fetal bovine serum (FBS) and 1% (v/v) penicillin/streptomycin, all purchased from PAN-Biotech GmbH, Aidenbach, Germany. HT29-MTX cells (clone ECACC 12040401; European Collection of Authenticated Cell Cultures, passages 60–72) were maintained in DMEM (Sigma-Aldrich, St. Louis, MO, USA). As supplements, 10% (v/v) of FBS, 1% (v/v) penicillin/streptomycin and 1% (v/v) non-essential amino acids, were used, all obtained from PAN-Biotech GmbH, Aidenbach, Germany. Both cell lines were cultured in 75-cm^2 tissue culture flasks in a humidified incubator at 37°C, with 5% CO_2. Culture medium was replaced every 2–3 days, and cells were routinely sub-cultured upon reaching approximately 80% confluence. To detach cells from the flasks,

culture medium was removed, and cells were washed twice with phosphate buffered saline - PBS (1x) (Gibco, ThermoFisher, MA, USA) followed by incubation with 0.25% (w/v) trypsin 2.21 mM EDTA solution (Corning, California, USA) in the CO_2 incubator for 5 min. The cell suspension was centrifuged at 150 x g for 5 min at room temperature (RT). Co-cultures of Caco-2 and HT29-MTX were seeded at a 9:1 ratio. The medium was changed every 2 to 3 days until completing 21 days of culture for differentiation.

2.3.1. Static cell cultures: inserts or 96-well plate

12-well plate inserts (cell-QART®; Northeim, Germany), in which the semi-permeable membrane is made of polyethylenterephthalate with a nominal thickness of 10 µm, provide a cell growth area of 1.12 cm² and feature 3 µm pores at a pore density of 1.7×10^6 pores•cm^{-2}. To avoid cell migration from the apical to the basolateral side, 250 µL of Matrigel (200 µg•mL^{-1}) diluted in DMEM free-serum was added to the cell culture inserts, incubated at room temperature for 2 h and then placed inside the 5% CO_2 incubator for 1 h to complete the polymerisation process. After trypsinization, the resulting pellet was resuspended in an appropriate volume of culture media to obtain a final cell density (1×10^5 cells•cm^{-2}), considering the surface area of a cell culture insert (1.12 cm^2) and using 500 µL of cell suspension per cell culture insert.

To assess the effect of fermentation supernatants on cell viability, cells were grown on 96-well plates for 21 days. After trypsinization, the resulting pellet was resuspended in an appropriate volume of culture media to obtain a final cell density (1×10^5 cells.cm^{-2}), considering the surface area of a well of 96-well plate (0.32 cm^2) and using 100 µL of cell suspension per well.

2.3.2. Dynamic cell cultures: Gut-chip

Caco-2 and HT29-MTX cells were seeded at $1 \cdot 10^5$ cells.cm^{-2} using 19.5 µL of cell suspension (1×10^6 cells·mL^{-1}) on the top of the ECM-coated membrane of the gut-chip. Cells were allowed to adhere overnight inside the CO_2 incubator and then the device was connected to a commercial 2-channel syringe pump using 12 mL syringes with an internal diameter of 15.9 mm, which perfused culture medium continuously through the upper and lower channels at a constant flow rate of 120 µL·h^{-1} for 7 days. In previous work, we have demonstrated that dynamic culture conditions significantly enhance epithelial cell differentiation, which is consistently achieved after 7 days in culture (Xavier et al. 2023).

2.4. Immunocytochemistry

The morphology of cells cultured on cell culture inserts or on-chip was assessed, through immunocytochemistry. Cells were washed with warm PBS (1x) and fixed with 4% paraformaldehyde (PFA) (ThermoFisher, Massachusetts, USA) in PBS (1x) for 15 min at RT. To permeabilize the cell and nuclear membranes, a solution of 0.2% Triton-X-100 (Sigma-Aldrich, St. Louis, MO, USA) was incubated for 10 min at 4°C and then, to minimize non-specific binding of antibodies, 2% bovine serum albumin (BSA) (Sigma-Aldrich, St. Louis, MO, USA) in PBS (1x) was incubated for at least 30 min at RT. Following

this, a solution of 5 μg·mL^{-1} Alexa Fluor® 488-conjugated occludin monoclonal antibody (AF488-Anti-Occludin; Thermo Fisher Scientific) and 0.1 μg•mL^{-1} phalloidin-TRITC (Sigma-Aldrich, St. Louis, MO, USA) were incubated overnight at 4°C. Cells were washed with PBS (1x) and a 1 μg·mL^{-1} of 4',6'-diamidino-2-phenylindole (DAPI) solution (Thermo Fisher Scientific, Waltham, MA, USA) was incubated for 10 min. The cells were mounted in Fluoroshield mounting media. Images were acquired using a Zeiss LSM780 confocal laser scanning microscope (Oberkochen, Germany) equipped with 405 nm and 561 nm diode lasers and a 488 nm argon laser and analysed using Zen 2010 software and ImageJ.

2.5. Transepithelial electrical resistance (TEER)

The intestinal epithelium barrier integrity was assessed using a Millicell ERS-2 Volt-ohmmeter with STX chopstick (Merck Millipore, Burlington, MA, USA) electrodes introduced simultaneously into the apical and basolateral compartments. For TEER evaluation, the well plates were taken out of the CO_2 incubator for 15 min, before the TEER measurement, to stabilise the culture medium's temperature and minimise variations. The TEER was calculated by subtracting the readings of the cell-free culture insert from the TEER reading with the cell monolayer and multiplying by the surface area of the membrane. Cell monolayers with a TEER over 500 Ω.cm^2 were considered tight monolayers and used for the experiments.

2.6. Apparent permeability (P_{app}) of Lucifer Yellow

The intestinal barrier integrity was assessed by measuring the apparent permeability (P_{app}) of Lucifer Yellow (Sigma-Aldrich, Darmstadt, Germany), a model molecule transported through the paracellular pathway. Lucifer yellow (50 μM in the vehicle) was introduced into the apical compartment (0.5 mL) while the basolateral compartment (1.5 mL) was filled with the vehicle. Every hour, up to 4 h, 100 μL samples were collected from the basolateral compartment to a 96-well plate, and fluorescence was measured using a microtiter plate reader with excitation/emission wavelengths of 428/540 nm. At the same time, a calibration curve was prepared through serial dilution of Lucifer yellow at initial concentration (50 μM) in the vehicle, in the range 0–6.25 μM. The apparent permeability coefficient of Lucifer Yellow was obtained through Eq. 1:

Equation 1 $P_{app} = \frac{dQ}{dt} \cdot \frac{V}{AC0}$

where dQ/dt is the permeability rate (μM·s^{-1}), which corresponds to the slope of the cumulative increase in the concentration of Lucifer Yellow in the basolateral chamber over time, V is the volume of the basolateral chamber (cm^3), A is the surface area (cm^2) and C0 is the initial concentration of Lucifer Yellow (μM) in the apical compartment.

2.7. Cell metabolic activity

Cell metabolic activity was evaluated through the resazurin (Sigma-Aldrich, Darmstadt, Germany) reduction assay. Caco-2/HT29-MTX co-cultures were seeded on 96-well plates and grown for 21 days.

Differentiated monolayers were exposed to fermentation supernatant at different dilutions (1:10 and 1:20) for 24 h and then replaced with 10 $\mu g \cdot mL^{-1}$ resazurin in complete MEM, for 3 h at 37°C. Complete culture medium (MEM) was used as a positive control and DMSO (40% v/v) (Sigma-Aldrich, Darmstadt, Germany) as a negative control. The cell metabolic activity was measured through the fluorescence signal obtained from the reduction reaction of resazurin to resorufin (λ_{ex} = 560 nm, λ_{em} = 590 nm), using a BioTeK® Synergy H1 (Winnoski, VT, USA) microplate reader. The results are expressed as a percentage of cell metabolic activity in relation to the positive control.

2.8. Gene expression analysis

2.8.1. RNA isolation and quantification

Total RNA was isolated with the RiboPure™ RNA Purification Kit following the manufacturer's instructions (Invitrogen™). Briefly, TRI Reagent™ was used to lyse cells and inactivate nucleases, and bromochloropropane was added for phase separation. The clear, aqueous phase, in which RNA partitioned, was collected and purified through a glass fibre filter. After purification, the eluted RNA was quantified using the Qubit™ RNA HS Assay Kit (Invitrogen™), and quality was evaluated by the A260/A280 ratio on NanoVue™ Plus Spectrophotometer.

2.8.2. RT-qPCR

cDNA synthesis was carried out according to the manufacturer's instructions, using TaqMan™ Reverse Transcription kit (Invitrogen™, Thermo Fisher Scientific, Waltham, MA, USA), where 135 ng of RNA was converted per condition. The RT reaction was performed on Veriti™ Thermal Cycler using the following parameters: a first incubation of 10 min at 25°C, transcription step of 30 min at 37°C, an inactivation step of 5 min at 95°C and a cool-down step until a 4°C temperature is reached. Real-Time PCR was performed using TaqMan™ Fast Advanced Master Mix (Applied Biosystems, Thermo Fisher Scientific, Waltham, MA, USA) and TaqMan™ gene expression assays (Applied Biosystems, Thermo Fisher Scientific, Waltham, MA, USA). For each condition, 4.5 ng of cDNA was used and run on StepOnePlus™ Real-Time PCR System (Thermo Fisher Scientific) with the following thermal protocol: 2 min at 50°C, 20 seconds at 95°C and 40 cycles of 1 second at 95°C and 20 seconds at 60°C for the denaturation and annealing steps, respectively. Relative gene expression levels were determined using the 2-ΔΔCT method, normalised to the housekeeping gene: glyceraldehyde-3-phosphate dehydrogenase (GAPDH). The following primers and probe were used: forward primer, 5'-CCAGGTGGTCTCCTCTGACTTC-3'; reverse primer, 5'-TCATACCAGGAAATGAGCTTGACA-3'; and TaqMan™ TAMRA probe, 5'-ACACCCACTCCTCCACCTTTGACGCT-3'. Occludin expression was determined using the TaqMan™ assay Hs05465837_g1.

2.9. Exposure of barrier-impaired Caco-2/HT29-MTX monolayers in cell culture inserts to fermentation supernatant

Barrier dysfunction is a hallmark of mucosal inflammation [26]. At day 21, barrier dysfunction was induced by exposing the intestinal epithelial monolayers to tumour necrosis factor alpha (TNF-α) (BioLegend, San Diego, California), a pro-inflammatory cytokine [27]. The culture medium was replaced with complete MEM in the apical compartment, and complete MEM containing TNF-α at a final concentration of 50 ng·mL^{-1} in the basolateral compartment, and cells were incubated for 48 h. Following this, the monolayers were exposed to distinct dilutions of fermented supernatants (1:10 and 1:20) to investigate their capacity to restore the intestinal barrier function. Budesonide (3 μM diluted in chloroform), a known anti-inflammatory compound (Sigma-Aldrich, Darmstadt, Germany) commonly used to treat inflammatory bowel disease (IBD) was used as a positive control [28]. Distinct vehicles were tested for the dilution of fermentation supernatant to determine the most suitable carrier: HBSS (PAN-Biotech, GmbH, Aidenbach, Germany), HBSS supplemented with 25 mM HEPES (Gibco, Thermo Fisher, MA, USA), complete MEM or MEM without FBS.

2.10. Statistical analysis

The Shapiro-Wilk test was used to analyse if the data followed a normal distribution. P-values were determined using a one-way analysis of variance (ANOVA) with Tukey's post- hoc test. Differences were considered statistically significant when * ($p < 0.05$), ** ($p < 0.005$), *** ($p < 0.001$) and **** ($p < 0.0001$). All data analysis and graphs were done using GraphPad Prism version 9.2.0 (GraphPad Software Inc., San Diego CA).

3. Results and discussion

3.1. Fermentation characterisation

3.1.1. Taxonomic profile and SCFA quantification

After 24 h of incubation under agitation and in anaerobic conditions, taxonomic profiling at the class level revealed similar microbial community structures between the two independent fermentations (sample 1 and sample 2), as shown in Fig. 1A. The communities were dominated by Clostridia (phylum Bacillota), accounting for approximately 43.0% of total reads in sample 1 and 39.2% in sample 2. Gammaproteobacteria represented another major class, comprising 31.1% of reads in sample 1 and 13.1% in sample 2. Similarly, Bacteroidia (phylum Bacteroidota) were detected at moderate levels in both samples, representing 5.3% of reads in sample 1 and 16.1% in sample 2. Members of the class Bacilli (phylum Bacillota) contributed to the microbial communities, accounting for 2.8% and 4.6% of reads in sample 1 and sample 2, respectively. Additional classes, including Negativicutes, Fusobacteriia, and Verrucomicrobiia, were present at lower relative abundances in both samples, each generally representing less than 6% of total reads. Several low-abundance taxa, including classes within Actinomycetota and other minor bacterial phyla, were detected at very low frequencies (< 1%) in both samples. A small proportion of reads remained unclassified at the class level. Overall, the class-level taxonomic profiles indicate that the two samples share a largely conserved microbial community

structure, with the same dominant bacterial classes present and broadly comparable relative abundance patterns.

Although Bacillota and Bacteroidota dominate *in vivo* (> 90% of gut bacteria) [29], batch faecal fermentations frequently deviate from this pattern, with Proteobacteria (including Gammaproteobacteria) becoming highly abundant after 24 h [30]. The observed Gammaproteobacteria levels in our fermentations are consistent with the lack of pH control, the accumulation of fermentation acids and the known *ex vivo* overgrowth tendencies of Enterobacteriaceae in simple media. Therefore, our results align with prior *in vitro* studies and likely reflect physicochemical constraints of the batch system (pH, buffering, substrate spectrum) rather than an artefactual or unique anomaly [31, 32]. This effect also impacted the concentration of the SCFA in the faecal supernatants. Bacillota, which include families like Lachnospiraceae and Ruminococcaceae, are significant producers of SCFAs, such as butyrate [33]. These SCFAs play a crucial role in maintaining gut health by serving as an energy source for colonocytes and having anti-inflammatory properties. Bacteroidota, on the other hand, are associated with the production of propionate [33, 34]. The balance and interaction between these phyla influence the overall production of SCFAs, impacting gut health and metabolic functions. After 24 h, acetate, propionate, and butyrate reached concentrations on the order of tens to a few hundred millimolar (after correcting for sampling dilution), which is comparable to the magnitude of SCFA concentrations reported in human colonic contents and faeces, where total SCFA typically range between ~ 70 and 140 mM in proximal colon and 10–70 mM in distal colon; individual SCFAs typically range from 8–40 mM (proximal) and 1–20 mM (distal), with acetate:propionate:butyrate ≈ 3:1:1 [35]. The relative distribution of acetate > propionate ≈ butyrate, together with measurable lactate and high formate, is consistent with metabolic profiles reported for faecal and in vitro colonic fermentations, acknowledging that closed batch cultures tend to accumulate higher SCFA levels than the *in vivo* colon due to the absence of absorption [36, 37]. After 24 h of *in vitro* anaerobic faecal fermentation, the levels of SCFA in the two fermentations were similar, with formic acid levels at 33000 $\mu g \cdot mL^{-1}$ (717 mM) approximately. Acetic acid represented the second most abundant SCFA in both samples, with concentrations in the range of 1500 $\mu g \cdot mL^{-1}$ (25 mM) approximately and lactic acid 3800 $\mu g \cdot mL^{-1}$ (42 mM). The lowest concentrations were observed for propionic and butyric acids, 300 $\mu g \cdot mL^{-1}$ (3.7-4.0 mM, respectively) and citric acid 550 $\mu g \cdot mL^{-1}$ (2.86 mM) (Fig. 1B). The total acid load and especially formate were clearly supra-physiological in the colonic context, therefore, 1:10 and 1:20 dilutions were conducted to (i) bring total SCFAs closer to *in vivo* ranges to avoid toxicity for the cells, (ii) avoid non-physiological toxicity/osmolarity on target cells, and (iii) cover a more realistic exposure range with a dose-response for downstream assays. After the dilutions, we had for 1:10 dilution concentrations of acetate ~ 2.5 mM, propionate/butyrate ~ 0.3–0.4 mM, and for 1:20 dilutions, concentrations of acetate ~ 1.3 mM, propionate/butyrate ~ 0.15–0.2 mM. These are at or below luminal levels, but they are within the range commonly used in cell culture and *ex vivo* experiments to mimic tissue exposure (Saleri et al., 2022).

3.2. Caco-2/HT29-MTX monolayers in cell culture inserts and on-chip

Caco-2/HT29-MTX (9:1 ratio) were grown in cell culture inserts for 21 days or in a microfluidic-based platform under continuous flow for 7 days. Confocal images demonstrated that cell cultures in inserts over 21 days resulted in cellular monolayers predominantly flattened, displaying a quasi-squamous morphology (Fig. 2A). In contrast, gut-chip cultures developed a 3D architecture within only 7 days of culture, more closely resembling the *in vivo* intestinal epithelium morphology (Fig. 2B). This accelerated acquisition of physiological morphology was accompanied by continuous TJ protein expression, also indicating functional differentiation under dynamic flow conditions. Together, these findings demonstrate that the gut-chip platform not only reduces differentiation time but also promotes the formation of structurally and functionally more relevant intestinal epithelial barriers compared with static cell culture systems.

As cells proliferate and differentiate, they form a continuous and tight monolayer, reflected in a progressive increase in the TEER [40]. Figure 3 shows a consistent increase in TEER values obtained from the Caco-2/HT29-MTX (9:1) cultures in cell culture inserts over the 21 days of differentiation.

TEER values reported in the literature for Caco-2/HT29-MTX co-cultures at the same 9:1 ratio vary considerably. Vincentini et al. reported TEER values of approximately 400 $\Omega.cm^2$, whereas Hilgendorf et al. and Pan et al. reported values of approximately 1800 and 250 $\Omega.cm^2$, respectively [41–43]. Such variability may reflect differences in experimental conditions and highlights the importance of controlling methodological factors, such as culture medium composition, cell passage number and temperature [16].

3.3. Exposure of Caco-2/HT29-MTX monolayers to fermentation supernatant

Two dilutions of the fermentation supernatant in HBSS, 1:10 and 1:20, were evaluated.

In cell culture inserts, after 21 days of culture, cells were washed with pre-warmed HBSS at 37°C. Fermentation products diluted in HBSS or solely HBSS (control) were added to the apical side (500 µL), while HBSS was used in the basolateral side (1500 µL). On-chip, following 7 days of culture, syringes were unplugged, and HBSS was flushed to wash remaining culture medium. The syringe containing fermentation supernatant, diluted in HBSS or in HBSS alone (control), was connected to the upper channel, and a syringe containing HBSS was connected to the bottom channel (Supplementary Material, Figure S1B). The flow of the pump was reduced to 20 $\mu L \cdot h^{-1}$ for 1 mL syringes with an internal diameter of 4.78 mm.

TEER was measured on day 21 of differentiation, immediately after replacing the culture medium (MEM) with fermentation supernatant diluted in HBSS. HBSS was used as the control condition. A slight decrease in TEER was observed at time 0 (Fig. 4A) compared with the values measured in MEM on day 21 before the medium change (Fig. 3). This decrease may be related to differences in the electrolyte composition and nutrient content of the two solutions [44]. MEM contains a broader range of nutrients and growth factors required for cell culture maintenance, whereas HBSS is a simpler balanced salt

solution. The change in the extracellular environment may therefore transiently affect the electrical resistance measured across the epithelial monolayer [45]. Following 4 h of exposure to the fermentation supernatant, TEER values showed an average increase compared with the values measured at 0 h (Fig. 4A).

Regarding the Lucifer Yellow permeability assay, at the end of the experiment (8 h) performed in cell culture inserts, neither the 1:10 nor the 1:20 fermentation supernatant dilutions resulted in a significant difference in P_{app} compared with the control group. These results indicate that, under the tested conditions, exposure to the fermentation supernatant did not significantly alter the permeability of the epithelial monolayer.

When comparing P_{app} of Lucifer Yellow in the HBSS control condition between the two models (Fig. 4B), P_{app} was consistently and significantly lower in cell culture inserts ($1.04 \times 10^{-7} \pm 8.98 \times 10^{-9}$ $cm.s^{-1}$) than in the dynamic gut-chip ($7.96 \times 10^{-7} \pm 1.82\ 10^{-7}$ $cm.s^{-1}$). The permeability measured in the cell culture inserts was also lower than the value reported in *ex vivo* studies using human samples in Ussing chambers (4.4×10^{-6} $cm.s^{-1}$)[46], suggesting that the static culture system may produce a less physiologically representative permeability profile.

In contrast, exposure to the fermentation supernatant in the dynamic gut-chip resulted in a significant reduction in Lucifer Yellow P_{app} compared with the control condition for both the 1:10 and 1:20 dilutions. This decrease in permeability suggests that the fermentation supernatant may enhance barrier function under the dynamic culture conditions tested, with a similar effect observed at both concentrations.

3.3.1. Testing vehicles for fermentation supernatant for longer exposure periods

To assess the effect of fermentation supernatant on cell viability following 24 h exposure in HBSS, Caco-2/HT29-MTX (9:1) co-cultures were established in 96-well plates and differentiated for 21 days. On day 21, differentiated cells were incubated for 24 h with complete MEM (positive control for cell viability), 40% DMSO (negative control), HBSS, fermentation supernatant diluted 1:10 in HBSS, or budesonide (3 µM) diluted in HBSS. Cell metabolic activity was subsequently assessed using the resazurin reduction assay (Fig. 5).

Cells exposed to budesonide (3 µM) diluted in HBSS or to HBSS showed a significant reduction in metabolic activity compared with the positive control (complete MEM), with decreases of more than 20% ($p < 0.001$). A more pronounced reduction of approximately 40% was observed following exposure to fermentation supernatant diluted 1:10 in HBSS ($p < 0.0001$). These results indicate that HBSS may not be a suitable carrier for fermentation supernatants during prolonged exposure, as incubation with HBSS for 24 h significantly reduced the metabolic activity of differentiated cells.

A 54% reduction in TEER was also observed following 24 h incubation with HBSS (Supplementary Material, Figure S2), further indicating that prolonged exposure to HBSS negatively affects epithelial barrier function. The reduction in both TEER and metabolic activity may be related to the limited nutrient content of HBSS compared with complete MEM, which becomes particularly relevant during prolonged incubation periods.

To identify alternative vehicles that could minimize these effects, complete MEM, MEM without FBS and HBSS supplemented with HEPES (25 mM) were evaluated [47]. Caco-2/HT29-MTX (9:1) co-cultures were grown on cell culture inserts for 21 days and subsequently incubated with each vehicle for 24 h. The relative TEER values, expressed with respect to the values measured on day 21 of culture, before and after the 24 h incubation period, are presented in Fig. 6.

As expected, the highest TEER values after 24 h of exposure were observed for complete MEM, followed by MEM without FBS and HBSS supplemented with 25 mM HEPES (HBSS-HEPES), whereas the lowest relative TEER values were observed for HBSS (Fig. 6). Compared with the TEER measured on day 21, exposure to HBSS resulted in a 54% decrease, while HBSS-HEPES resulted in an approximately 25% decrease. In contrast, exposure to MEM without FBS and complete MEM resulted in an increase in TEER with statistically significant differences. Although MEM without FBS maintained the epithelial barrier more effectively than the other tested vehicles, its complex composition may introduce additional factors that could influence permeability measurements. Therefore, considering the intended application as a carrier for fermentation supernatants in permeability studies, HBSS-HEPES was selected as an alternative vehicle that provides a simpler composition while maintaining epithelial barrier function and cell metabolic activity.

The effects of HBSS-HEPES, fermentation supernatant diluted 1:10 or 1:20 in HBSS-HEPES), and budesonide (3 μM in HBSS-HEPES) on cell metabolic activity were subsequently assessed using the resazurin reduction assay (Supplementary Material, Figure S3). After 24 h of incubation, neither fermentation supernatant dilution nor budesonide significantly affected the metabolic activity of differentiated Caco-2/HT29-MTX co-cultures compared with complete MEM. Metabolic activity remained comparable to that observed in cells exposed to complete MEM under all tested conditions, with no statistically significant differences detected.

3.4. Exposure of barrier-impaired Caco-2/HT29-MTX monolayers in cell culture inserts to fermentation supernatant

To evaluate the effect of the fermentation supernatant on a compromised intestinal epithelial barrier, differentiated Caco-2/HT29-MTX monolayers were first exposed to TNF-α (50 ng·mL^{-1}) in the basolateral compartment on day 21 of culture for 48 h to induce barrier dysfunction. Subsequently, cells were exposed to fermentation supernatant diluted 1:10 or 1:20 in HBSS-HEPES, or to budesonide (3 μM in HBSS-HEPES), for 24 h, as shown in Fig. 7A. The barrier integrity was assessed by measuring TEER

before and after TNF-α exposure and following treatment with the fermentation supernatant or budesonide. In addition, P_{app} of Lucifer Yellow was determined following the 24 h treatment period. To further assess the effects of the fermentation supernatant on TJ regulation, occludin gene expression was quantified in TNF-challenged cells, before and after treatment with the fermentation supernatant or budesonide. Figure 7B shows the relative TEER values, expressed with respect to the value measured on day 21 of culture, before TNF-α exposure (day 21), after the 48 h TNF-α challenge (day 23), and following the subsequent 24 h incubation with HBSS-HEPES, fermentation supernatant diluted 1:10 or 1:20 in HBSS-HEPES, or budesonide (3 mM in HBSS-HEPES) (day 24).

TEER measurements showed that exposure to the inflammatory stimulus for 48 h in the basolateral compartment resulted in an approximately 45% decrease in TEER compared with the pre-challenge values (Fig. 7B ii-v). Le *et al.* reported that a decrease in TEER of at least 25% can be used as an indicator of an inflamed intestinal epithelial model (Le et al., 2023), supporting the establishment of a barrier-impaired condition in the present study. Following incubation with the fermentation supernatant, both dilutions (1:10 and 1:20 in HBSS-HEPES) resulted in a recovery of TEER to values comparable to those measured before TNF-α exposure (Fig. 7B iii and iv). A similar recovery of barrier function was observed following treatment with budesonide (3 μM in HBSS-HEPES) (Fig. 7B, v). These results suggest that the fermentation supernatant was able to improve barrier function under the TNF-α-induced compromised condition, with comparable responses observed for both dilutions.

Following treatment with fermentation supernatant diluted 1:10 or 1:20 in HBSS-HEPES, Papp values were not significantly different from those measured in the healthy control condition. A similar response was observed following treatment with budesonide (3 μM in HBSS-HEPES). These results indicate that that exposure to the fermentation supernatant under the conditions tested was associated with a reduction in the increased permeability observed following TNF-α challenge, suggesting a potential beneficial effect on barrier function under compromised conditions. However, the absence of a significant difference from the healthy control does not by itself establish an anti-inflammatory mechanism or demonstrate complete recovery of the epithelial barrier. Overall, the results support the suitability of the fermentation supernatant approach for investigating the modulation of intestinal barrier function under TNF-α-induced barrier dysfunction.

Figure 8B shows a reduction in occluding gene expression in the TNF-α-challenged condition compared with the healthy control, although the difference was not statistically significant. Reduced occludin expression has previously been reported in models of intestinal inflammation [50], consistent with the observed trend in the present study. This finding further supports the involvement of TJ regulation in the maintenance of intestinal epithelial barrier function. Interestingly, occludin expression was also reduced following treatment with budesonide (3 μM in HBSS-HEPES), despite the reported anti-inflammatory and barrier-modulating effects of this drug (Becker et al., 2023). This unexpected finding may reflect differences between the regulation of occludin gene expression and functional barrier responses, as well as the specific experimental conditions used in the present study. Further investigation would be required to determine the mechanisms underlying this response.

4. Conclusion

Overall, this study demonstrates the feasibility of using faecal fermentation supernatants to investigate the effects of complex microbiota-derived products on intestinal epithelial barrier function. Under the conditions tested, the fermentation supernatant did not compromise barrier function in healthy Caco-2/HT29-MTX monolayers, supporting its use as an alternative approach to direct microbiota-epithelial co-culture. Comparison between static cell culture inserts and the dynamic gut-chip revealed marked differences in epithelial permeability, with higher Lucifer Yellow permeability observed under dynamic culture conditions. The permeability measured in the dynamic gut-chip was closer to values reported in *ex vivo* studies using human samples in Ussing chambers, whereas static cultures exhibited lower permeability. These findings highlight the influence of the culture platform on the assessment of epithelial barrier function and support the use of dynamic models when a more physiologically representative permeability profile is required.

The study also demonstrated the importance of carefully selecting the carrier and exposure conditions. HBSS was not suitable for prolonged exposure, as it negatively affected both cell metabolic activity and barrier function, whereas HBSS-HEPES provided a more suitable carrier for 24 h incubations while maintaining cell viability and barrier function. These findings emphasise that vehicle-related effects should be considered when designing experiments involving prolonged exposure of intestinal epithelial models.

Importantly, treatment with fermentation supernatant following TNF-α-induced barrier dysfunction was associated with a reduction in the increased epithelial permeability, with P_{app} values becoming comparable to those of the healthy control condition. These findings provide a basis for evaluating fermentation-derived products using cell-based intestinal models and establish experimental conditions that can be applied to samples generated throughout the fermentation process. In particular, the approach can be used to investigate real fermentation samples, such as upstream digesta or other fermentation-derived fractions, and to assess their effects on intestinal epithelial barrier function under both healthy and barrier-impaired conditions.

Taken together, this work provides a practical *in vitro* strategy for evaluating faecal fermentation samples using intestinal epithelial models representing both healthy and barrier-impaired conditions. The findings highlight the importance of considering the culture platform, carrier composition, and exposure duration when assessing the effects of complex microbiota-derived products. The experimental framework established here can therefore serve as a basis for the systematic testing of different fermentation samples and for subsequent mechanistic investigations using physiologically relevant intestinal *in vitro* models.

Declarations

Ethics statement

The Clinical Research Ethics Committee of the Cork Teaching Hospitals, UCC, approved the study (ECM 4 (mm) 09/03/2021) and faecal samples from healthy donors without antibiotic treatment in the previous six months were collected after written consent.

Additional information

Authors declared no conflicts of interest.

Funding

This work was supported by Enterprise Ireland and the European Union's Horizon 2020 research and innovation programme under the Marie Skłodowska-Curie grant agreement number 847402 awarded to EG-G, who was also funded by a Beatriz Galindo scholarship from the Spanish Ministry of Universities [BG22/00060]. Research in the group of PDC is funded through Science Foundation Ireland (SFI) under grant number [SFI/12/RC/2273] (APC Microbiome Ireland), and SFI together with the Irish Department of Agriculture, Food and the Marine, [SFI/16/RC/3835] (VistaMilk), by the Enterprise Ireland funded Food Health Ireland project and by the European Commission under the Horizon 2020 program under grant numbers [101060218] (DOMINO) and [101084642] (Co-Diet). MDN acknowledges the financial support by the Portuguese Foundation for Science and Technology (FCT) through her Doctoral Grant with the following reference 2023.00216.BD and DOI identifier https://doi.org/10.54499/2023.00216.BD.

Author Contribution

Sofia Sousa: Investigation, Methodology, Formal analysis, Data Curation, Formal Analysis, Visualisation, Writing – original draft; Patrícia Rodrigues: Investigation, Methodology, Formal analysis, Data Curation, Formal Analysis, Visualisation, Writing – original draft; Verônica Morato: Investigation, Data Curation, Formal Analysis, Visualisation, Writing – review & editing; Mafalda Neto: Investigation, Methodology, Validation, Data Curation, Formal Analysis, Visualisation, Writing – review & editing; Enriqueta Garcia-Gutierrez: Conceptualization, Investigation, Methodology, Validation, Data Curation, Formal Analysis, Visualisation, Writing – review & editing; Victor Calero: Conceptualization, Supervision, Writing – review & editing, Paul D. Cotter: Funding acquisition, Writing – review & editing; Lorenzo Pastrana: Funding acquisition, Writing – review & editing; Catarina Gonçalves: Conceptualization, Methodology, Supervision, Validation, Funding acquisition, Writing – review & editing.

Acknowledgement

The authors want to thank Helen Slattery for her support on SCFA analyses, Dr. Fiona Crispie and Dr. Gaston Allendez for sample sequencing. M.D.N. acknowledges the financial support by the Portuguese Foundation for Science and Technology (FCT) through her Doctoral Grant with the following reference 2023.00216.BD and DOI identifier https://doi.org/10.54499/2023.00216.BD. V.C. acknowledges funding from the European Union's Horizon Europe research and innovation programme under the Marie Sklodowska-Curie grant agreement No 101153594.

Data Availability

Sequencing data are publicly available in the European Nucleotide Archive (ENA), accession number PRJEB128142. Raw data and analysis files of the faecal sample sequencing are available at https://github.com/enriquetagarcia/barrier-integrity-gut-on-a-chip.

CRediT authorship contribution statement

Sofia Sousa: Investigation, Methodology, Formal analysis, Data Curation, Formal Analysis, Visualisation, Writing – original draft; **Patrícia Rodrigues**: Investigation, Methodology, Formal analysis, Data Curation, Formal Analysis, Visualisation, Writing – original draft; **Verônica Morato**: Investigation, Data Curation, Formal Analysis, Visualisation, Writing – review & editing; **Mafalda Neto**: Investigation, Methodology, Validation, Data Curation, Formal Analysis, Visualisation, Writing – review & editing; **Enriqueta Garcia-Gutierrez**: Conceptualization, Investigation, Methodology, Validation, Data Curation, Formal Analysis, Visualisation, Writing – review & editing; **Victor Calero**: Conceptualization, Supervision, Writing – review & editing, **Paul D. Cotter**: Funding acquisition, Writing – review & editing; **Lorenzo Pastrana**: Funding acquisition, Writing – review & editing; **Catarina Gonçalves**: Conceptualization, Methodology, Supervision, Validation, Funding acquisition, Writing – review & editing.

References

1. Chen, S. et al. Energy metabolism and the intestinal barrier: implications for understanding and managing intestinal diseases. *Frontiers in Microbiology* vol. 16 Preprint at (2025). https://doi.org/10.3389/fmicb.2025.1515364
2. Lin, P. Y., Stern, A., Peng, H. H., Chen, J. H. & Yang, H. C. Redox and Metabolic Regulation of Intestinal Barrier Function and Associated Disorders. *International Journal of Molecular Sciences* vol. 23 Preprint at (2022). https://doi.org/10.3390/ijms232214463
3. Macedo, M. H., Dias Neto, M., Pastrana, L., Gonçalves, C. & Xavier, M. Recent Advances in Cell-Based In Vitro Models to Recreate Human Intestinal Inflammation. *Advanced Science* vol. 10 Preprint at (2023). https://doi.org/10.1002/advs.202301391
4. Thursby, E. & Juge, N. Introduction to the human gut microbiota. *Biochemical Journal* vol. 474 1823–1836 Preprint at (2017). https://doi.org/10.1042/BCJ20160510

5. Ney, L. M. et al. Short chain fatty acids: key regulators of the local and systemic immune response in inflammatory diseases and infections. *Open Biology* vol. 13 Preprint at (2023). https://doi.org/10.1098/rsob.230014
6. Xiong, R. G. et al. Health Benefits and Side Effects of Short-Chain Fatty Acids. *Foods* vol. 11 Preprint at (2022). https://doi.org/10.3390/foods11182863
7. He, J. et al. Short-chain fatty acids and their association with signalling pathways in inflammation, glucose and lipid metabolism. *International Journal of Molecular Sciences* vol. 21 1–16 Preprint at (2020). https://doi.org/10.3390/ijms21176356
8. Bilotta, A. J. & Cong, Y. Gut microbiota metabolite regulation of host defenses at mucosal surfaces: Implication in precision medicine. *Precision Clinical Medicine* vol. 2 110–119 Preprint at (2019). https://doi.org/10.1093/pcmedi/pbz008
9. Silva, Y. P., Bernardi, A. & Frozza, R. L. The Role of Short-Chain Fatty Acids From Gut Microbiota in Gut-Brain Communication. *Frontiers in Endocrinology* vol. 11 Preprint at (2020). https://doi.org/10.3389/fendo.2020.00025
10. Ma, J., Piao, X., Mahfuz, S., Long, S. & Wang, J. The interaction among gut microbes, the intestinal barrier and short chain fatty acids. *Animal Nutrition* vol. 9 159–174 Preprint at (2022). https://doi.org/10.1016/j.aninu.2021.09.012
11. Gill, P. A., van Zelm, M. C., Muir, J. G. & Gibson, P. R. Review article: short chain fatty acids as potential therapeutic agents in human gastrointestinal and inflammatory disorders. *Alimentary Pharmacology and Therapeutics* vol. 48 15–34 Preprint at (2018). https://doi.org/10.1111/apt.14689
12. Sun, Y. & O'Riordan, M. X. D. Regulation of bacterial pathogenesis by intestinal short-chain fatty acids. in *Advances in Applied Microbiology* vol. 85 93–118Academic Press Inc., (2013).
13. Moutinho, S. Researchers and regulators plan for a future without lab animals. *Nature Medicine* vol. 29 2151–2154 Preprint at (2023). https://doi.org/10.1038/s41591-023-02362-z
14. Joshi, A., Soni, A. & Acharya, S. In vitro models and ex vivo systems used in inflammatory bowel disease. *vitro models*. **1**, 213–227 (2022).
15. Haddad, M. J. et al. Complexification of In Vitro Models of Intestinal Barriers, A True Challenge for a More Accurate Alternative Approach. *International Journal of Molecular Sciences* vol. 24 Preprint at (2023). https://doi.org/10.3390/ijms24043595
16. Darling, N. J., Mobbs, C. L., González-Hau, A. L., Freer, M. & Przyborski, S. Bioengineering Novel in vitro Co-culture Models That Represent the Human Intestinal Mucosa With Improved Caco-2 Structure and Barrier Function. *Front Bioeng. Biotechnol* **8**, (2020).
17. Fedi, A. et al. In vitro models replicating the human intestinal epithelium for absorption and metabolism studies: A systematic review. *Journal of Controlled Release* vol. 335 247–268 Preprint at (2021). https://doi.org/10.1016/j.jconrel.2021.05.028
18. Park, G. S. et al. Emulating Host-Microbiome Ecosystem of Human Gastrointestinal Tract in Vitro. *Stem Cell. Rev. Rep.* **13**, 321–334 (2017).

19. Donkers, J. M., van der Vaart, J. I. & van de Steeg, E. Gut-on-a-Chip Research for Drug Development: Implications of Chip Design on Preclinical Oral Bioavailability or Intestinal Disease Studies. *Biomimetics* vol. 8 Preprint at (2023). https://doi.org/10.3390/biomimetics8020226
20. Xavier, M. et al. From mouth to gut: microfluidic in vitro simulation of human gastro-intestinal digestion and intestinal permeability. *Analyst* **148**, 3193–3203 (2023).
21. Akhtar, M. et al. Gut microbiota-derived short chain fatty acids are potential mediators in gut inflammation. *Animal Nutrition* vol. 8 350–360 Preprint at (2022). https://doi.org/10.1016/j.aninu.2021.11.005
22. O'Donnell, M. M. et al. Preparation of a standardised faecal slurry for ex-vivo microbiota studies which reduces inter-individual donor bias. *J. Microbiol. Methods*. **129**, 109–116 (2016).
23. Fooks, L. J. & Gibson, G. R. Mixed culture fermentation studies on the effects of synbiotics on the human intestinal pathogens Campylobacter jejuni and Escherichia coli. *Anaerobe* **9**, 231–242 (2003).
24. Volant, S. et al. SHAMAN: A user-friendly website for metataxonomic analysis from raw reads to statistical analysis. *BMC Bioinformatics* **21**, (2020).
25. Guerrini, C. J., Botkin, J. R. & McGuire, A. L. Clarify the HIPAA right of access to individuals' research data. *Nature Biotechnology* vol. 37 850–852 Preprint at (2019). https://doi.org/10.1038/s41587-019-0190-3
26. Lechuga, S., Braga-Neto, M. B., Naydenov, N. G., Rieder, F. & Ivanov, A. I. Understanding disruption of the gut barrier during inflammation: Should we abandon traditional epithelial cell lines and switch to intestinal organoids? *Frontiers in Immunology* vol. 14 Preprint at (2023). https://doi.org/10.3389/fimmu.2023.1108289
27. Gijzen, L. et al. An Intestine-on-a-Chip Model of Plug-and-Play Modularity to Study Inflammatory Processes. *SLAS Technol.* **25**, 585–597 (2020).
28. Becker, H. E. F., Demers, K., Derijks, L. J. J., Jonkers, D. M. A. E. & Penders, J. Current evidence and clinical relevance of drug-microbiota interactions in inflammatory bowel disease. *Frontiers in Microbiology* vol. 14 Preprint at (2023). https://doi.org/10.3389/fmicb.2023.1107976
29. Stojanov, S., Berlec, A. & Štrukelj, B. The influence of probiotics on the firmicutes/bacteroidetes ratio in the treatment of obesity and inflammatory bowel disease. *Microorganisms* vol. 8 1–16 Preprint at (2020). https://doi.org/10.3390/microorganisms8111715
30. Takagi, R. et al. A single-batch fermentation system to simulate human colonic microbiota for high-throughput evaluation of prebiotics. *PLoS One* **11**, (2016).
31. Esra Ilhan, Z., Marcus, A. K., Kang, D. W., Rittmann, B. E. & Krajmalnik-Brown, R. pH-Mediated Microbial and Metabolic Interactions in Fecal Enrichment Cultures. (2017). https://doi.org/10.1128/mSphere doi:10.1128/mSphere.
32. Mathur, H. et al. Methods to mitigate Escherichia coli blooms in human ex vivo colon model experiments using the high throughput micro-Matrix bioreactor fermentation system. *MethodsX* **11**, 102393 (2023).

33. Jackson, R., Yao, T., Bulut, N., Cantu-Jungles, T. M. & Hamaker, B. R. Protein combined with certain dietary fibers increases butyrate production in gut microbiota fermentation. *Food Funct.* **15**, 3186–3198 (2024).
34. Döring, C. & Basen, M. Propionate production by Bacteroidia gut bacteria and its dependence on substrate concentrations differs among species. *Biotechnology Biofuels Bioproducts* **17**, (2024).
35. Topping, D. L. & Clifton, P. M. *Short-Chain Fatty Acids and Human Colonic Function: Roles of Resistant Starch and Nonstarch Polysaccharides*. (2001). http://physrev.physiology.org
36. Liebisch, G. et al. Quantification of fecal short chain fatty acids by liquid chromatography tandem mass spectrometry—investigation of pre-analytic stability. *Biomolecules* **9**, (2019).
37. Rahat-Rozenbloom, S., Fernandes, J., Gloor, G. B. & Wolever, T. M. S. Evidence for greater production of colonic short-chain fatty acids in overweight than lean humans. *Int. J. Obes.* **38**, 1525–1531 (2014).
38. Saleri, R. et al. Effects of different short-chain fatty acids (SCFA) on gene expression of proteins involved in barrier function in IPEC-J2. *Porcine Health Manag* **8**, (2022).
39. Xiong, R. G. et al. Health Benefits and Side Effects of Short-Chain Fatty Acids. *Foods* vol. 11 Preprint at (2022). https://doi.org/10.3390/foods11182863
40. Felix, K., Tobias, S., Jan, H., Nicolas, S. & Michael, M. Measurements of transepithelial electrical resistance (TEER) are affected by junctional length in immature epithelial monolayers. *Histochem. Cell. Biol.* https://doi.org/10.1007/s00418-021-02026-4 (2021).
41. Hilgendorf, C. et al. Caco-2 versus Caco-2/HT29-MTX Co-cultured Cell Lines: Permeabilities Via Diffusion, Inside- and Outside-Directed Carrier-Mediated Transport. *J. Pharm. Sci.* **89**, 63–75 (2000).
42. Pan, F., Han, L., Zhang, Y., Yu, Y. & Liu, J. Optimization of Caco-2 and HT29 co-culture *in vitro* cell models for permeability studies. *Int. J. Food Sci. Nutr.* **66**, 680–685 (2015).
43. Vincentini, O. et al. Towards the Standardization of Intestinal In Vitro Advanced Barrier Model for Nanoparticles Uptake and Crossing: The SiO2 Case Study. *Cells* **11**, 3357 (2022).
44. Tu, K. H. et al. Development of Real-Time Transendothelial Electrical Resistance Monitoring for an In Vitro Blood-Brain Barrier System. *Micromachines (Basel)*. **12**, 37 (2020).
45. Bunchongprasert, K. & Shao, J. Impact of Media in Transport Study on Cell Monolayer Integrity and Permeability. *J. Pharm. Sci.* **109**, 1145–1152 (2020).
46. Rozehnal, V. et al. Human small intestinal and colonic tissue mounted in the Ussing chamber as a tool for characterizing the intestinal absorption of drugs. *Eur. J. Pharm. Sci.* **46**, 367–373 (2012).
47. Ingels, F. et al. *Simulated Intestinal Fluid as Transport Medium in the Caco-2 Cell Culture Model*. *International J. Pharmaceutics* **232** (2002).
48. Le, N. P. K., Altenburger, M. J. & Lamy, E. Development of an Inflammation-Triggered In Vitro Leaky Gut Model Using Caco-2/HT29-MTX-E12 Combined with Macrophage-like THP-1 Cells or Primary Human-Derived Macrophages. *Int J. Mol. Sci* **24**, (2023).

49. de Ponce, M. C., Guyot, J. P. & Laurent-Babot, C. Intestinal in vitro cell culture models and their potential to study the effect of food components on intestinal inflammation. *Critical Reviews in Food Science and Nutrition* vol. 59 3648–3666 Preprint at (2019). https://doi.org/10.1080/10408398.2018.1506734
50. Chelakkot, C., Ghim, J. & Ryu, S. H. Mechanisms regulating intestinal barrier integrity and its pathological implications. *Experimental and Molecular Medicine* vol. 50 Preprint at (2018). https://doi.org/10.1038/s12276-018-0126-x

Figures

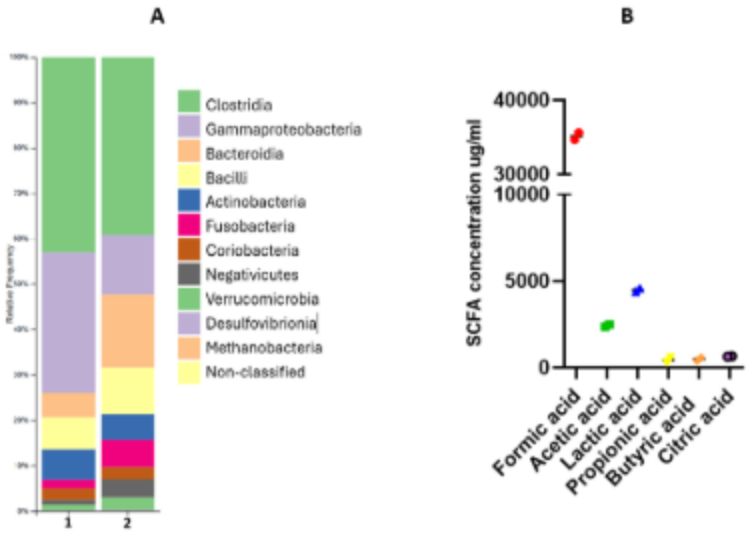


Figure 1

(A) Class-level taxonomic composition of bacterial communities.
Stacked bar plots show the relative abundance (%) of bacterial classes in both samples (1 and 2) generated using the taxa bar plot visualisation in QIIME 2. The two samples display highly similar class-level community profiles. **(B)** Short-chain fatty acids (SCFAs) concentrations ($\mu g \times mL^{-1}$): formic, acetic, lactic, propionic, butyric, and citric acids obtained in both samples. Each point represents an individual measurement.

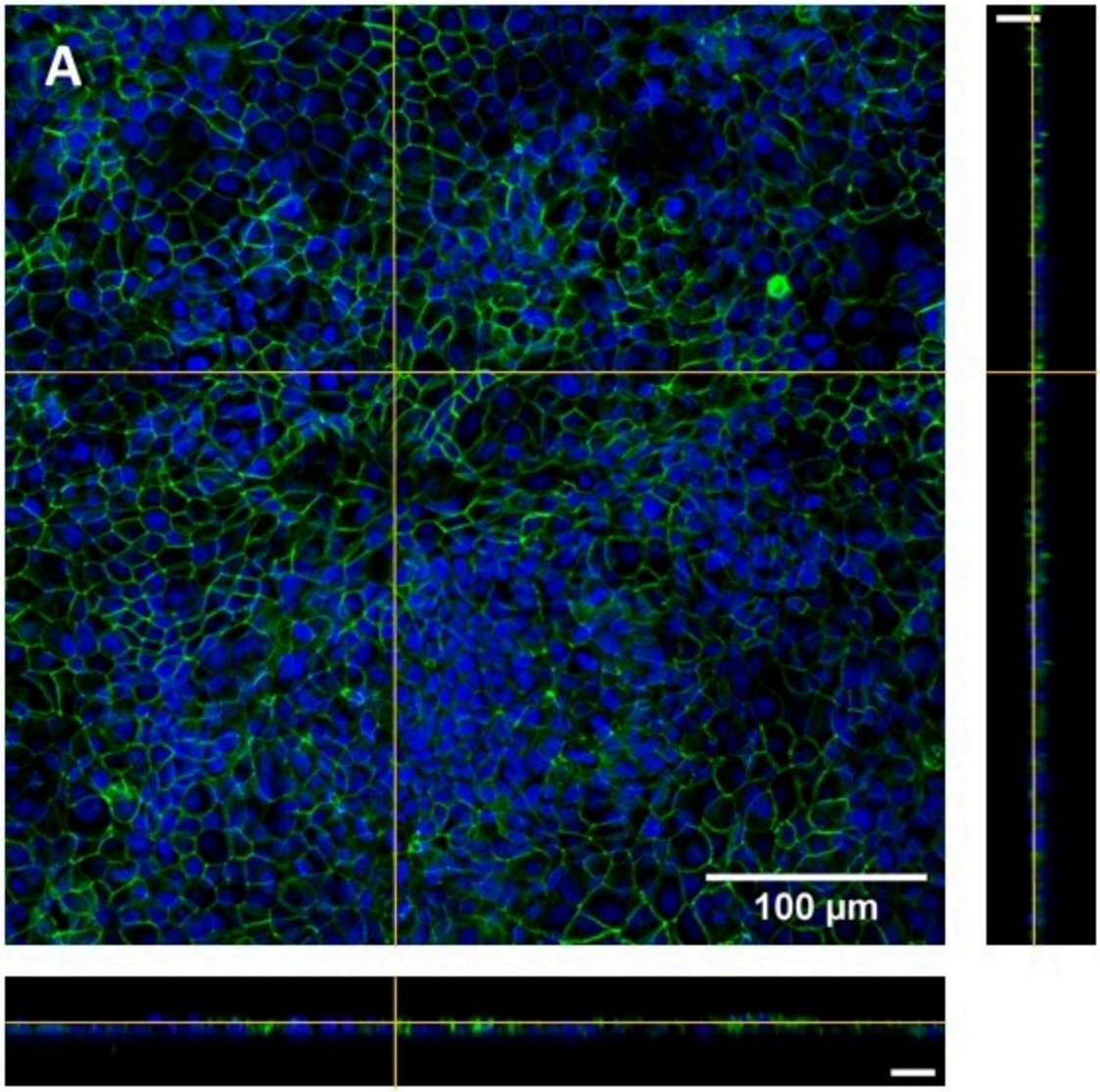


Figure 2

Confocal images and orthogonal cross-section views of occludin (green), and nuclei (blue) of Caco-2/HT29-MTX monolayers grown on **(A)** cell culture inserts for 21 days, and **(B)** on-chip under 7 days of continuous flow (120 µL·h^{-1}). The bar in the orthogonal views corresponds to 20 µm.

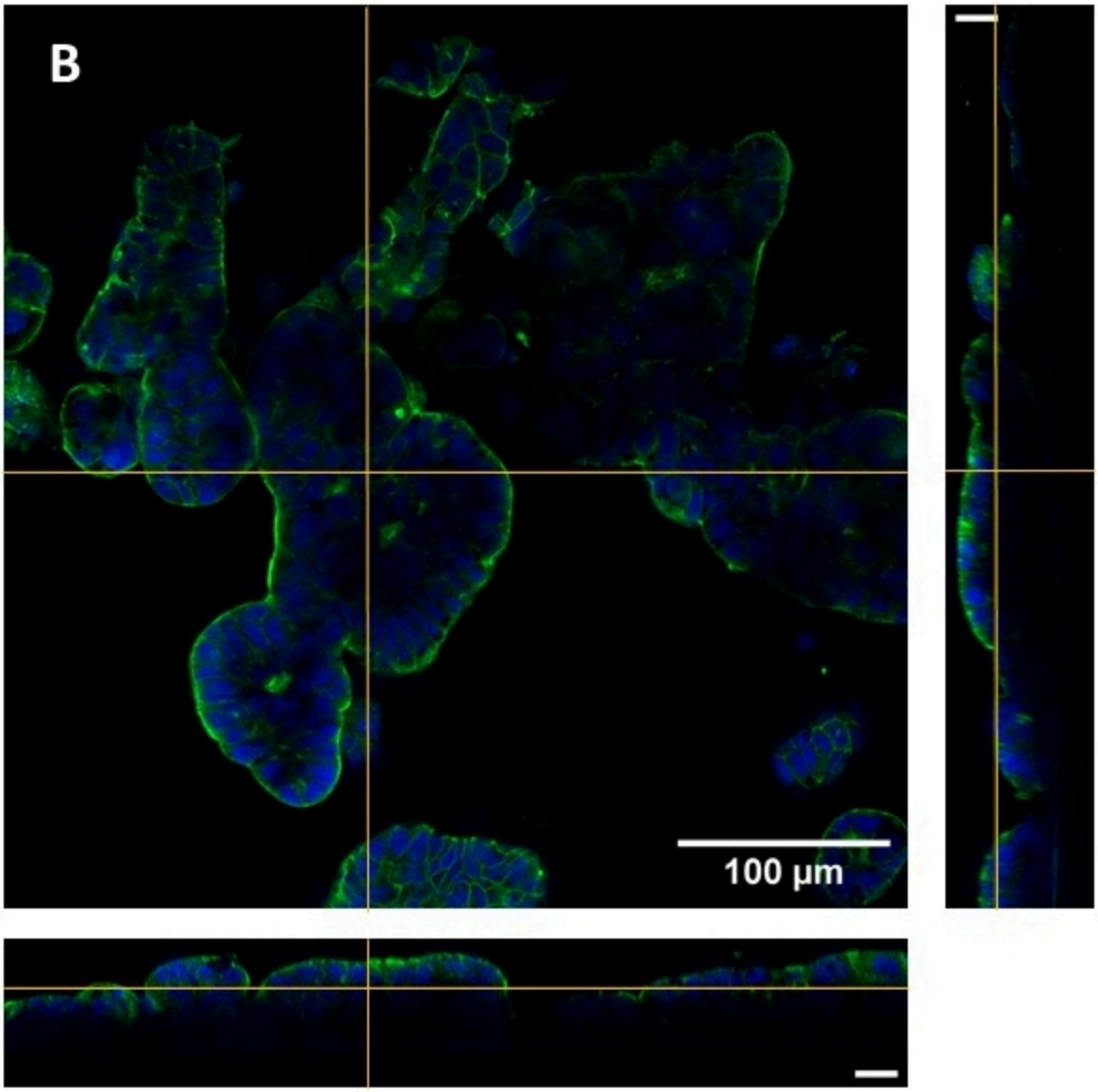


Figure 3

TEER of Caco-2/HT29-MTX (9:1) co-cultures over 21 days of culture in cell culture inserts. Values are presented as mean ± SD; N=3 independent experiments, with n=4 technical replicates per experiment.

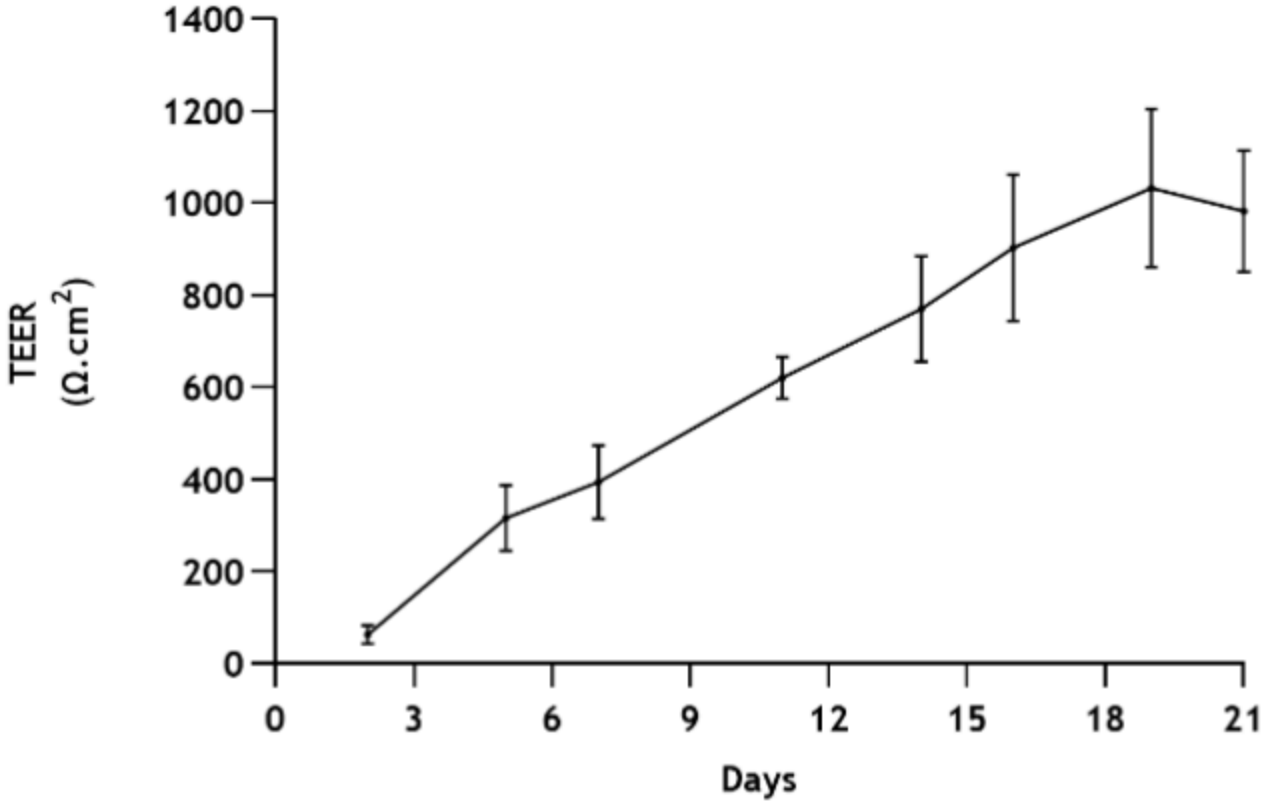


Figure 4

(A) TEER values measured immediately after exposure to the fermentation supernatant (0 h), after 4 h of exposure (4 h), and during the Lucifer Yellow permeability assay (5-8 h). **(B)** Apparent permeability (P_{app}) of Lucifer Yellow in Caco-2/HT29-MTX monolayers grown under static and dynamic conditions in HBSS (control) or exposed to fermentation supernatant diluted in HBSS. Values are presented as mean ± SD; n ≥ 4. Statistical significance is indicated by * ($p < 0.05$), ** ($p < 0.005$) and **** ($p < 0.0001$).

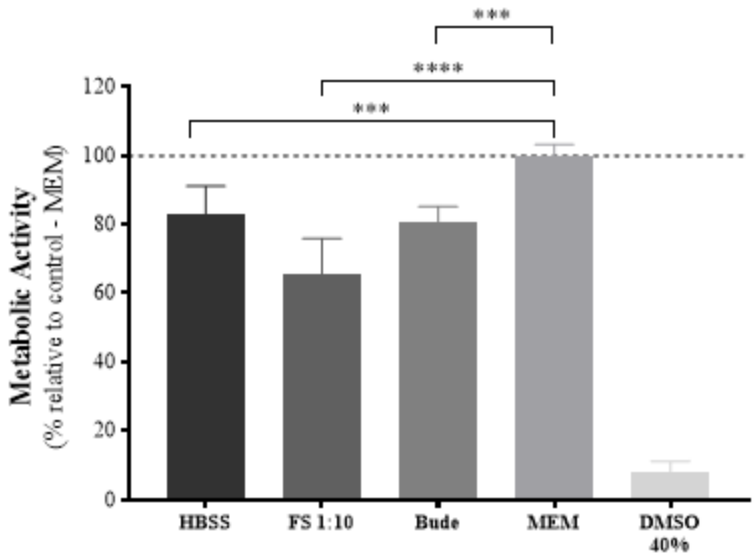


Figure 5

Relative TEER of differentiated Caco-2/ HT29-MTX (9:1) monolayers when incubated with **(A)** complete MEM, **(B)** MEM without FBS, **(C)**HBSS, or **(D)** HBSS-HEPES. TEER values are expressed relative to the value measured on day 21 of culture. Values are presented as mean ± SD; n ≥ 4. Statistical significance is indicated by *** ($p < 0.001$) and **** ($p < 0.0001$).

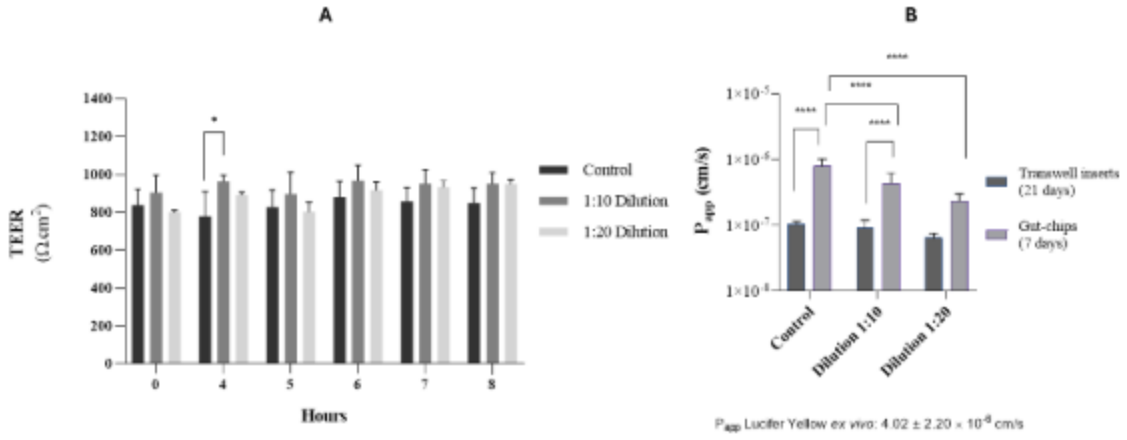


Figure 6

Cell metabolic activity assessed using the resazurin reduction assay in Caco-2/HT29-MTX co-cultures grown in 96-well plates for 21 days. On day 21, cells were exposed to MEM (positive control), HBSS, fermentation supernatant diluted 1:10 in HBSS, or budesonide (3 mM) for 24 h. 40 % DMSO was used as the negative control. Values are presented as mean ± SD; N = 2 independent experiments, with n = 3 technical replicates per experiment. Statistical significance is indicated by *** ($p < 0.001$) and **** ($p < 0.0001$).

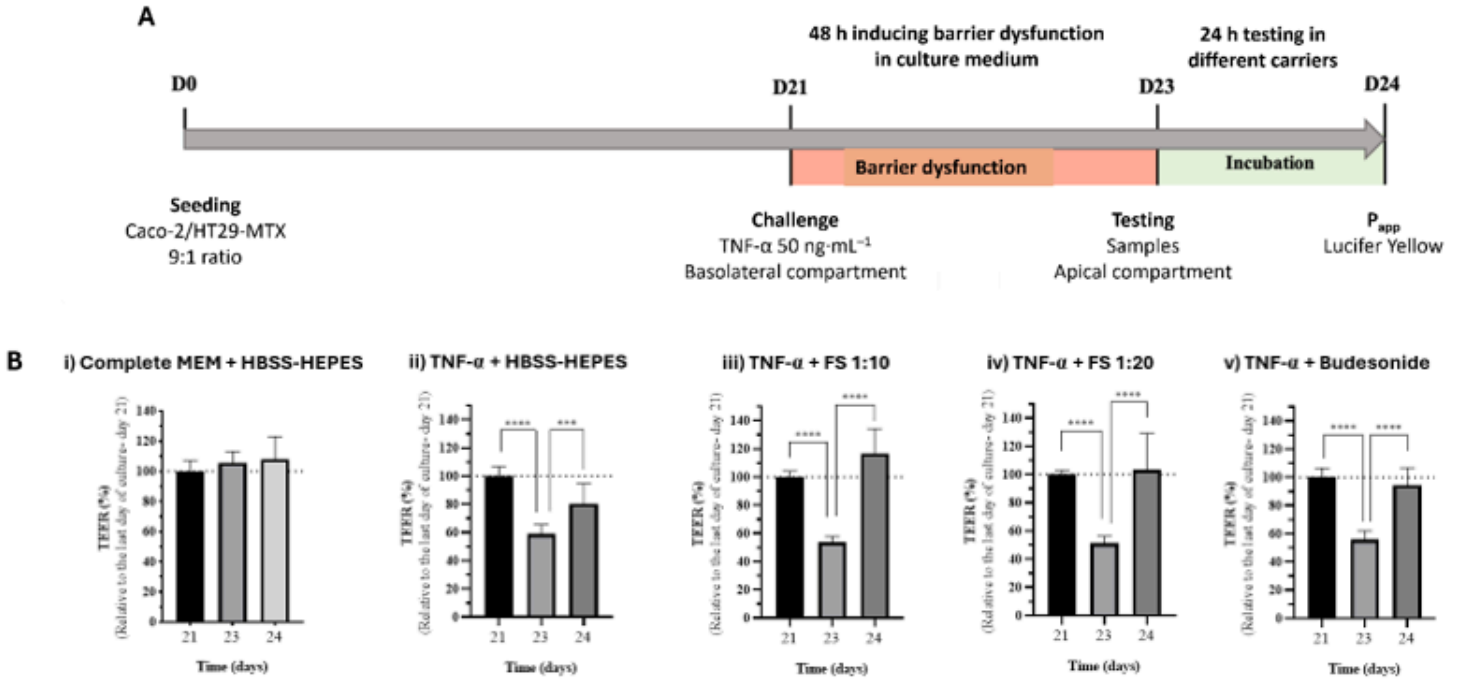


Figure 7

(A) Experimental timeline showing cell seeding, induction of barrier dysfunction, and exposure to the different treatments. Caco-2/HT29-MTX (9:1) co-cultures were grown on cell culture inserts for 21 days. **(B)** Relative TEER, expressed with respect to the value measured on day 21 of culture, following exposure to **i)** complete MEM or **(ii-v)** TNF-a (50 ng×mL^{-1}) in the culture medium for 48 h, followed by 24 h incubation with **(i-ii)** HBSS-HEPES, fermentation supernatant diluted in HBSS-HEPES at **(iii)** 1:10 or **(iv)** 1:20, or **(v)** budesonide (3 mM in HBSS-HEPES). Values are presented as mean ± SD; N=3 independent experiments, with n=4 technical replicates per experiment. Statistical significance is indicated by *** ($p < 0.001$) and **** ($p < 0.0001$).

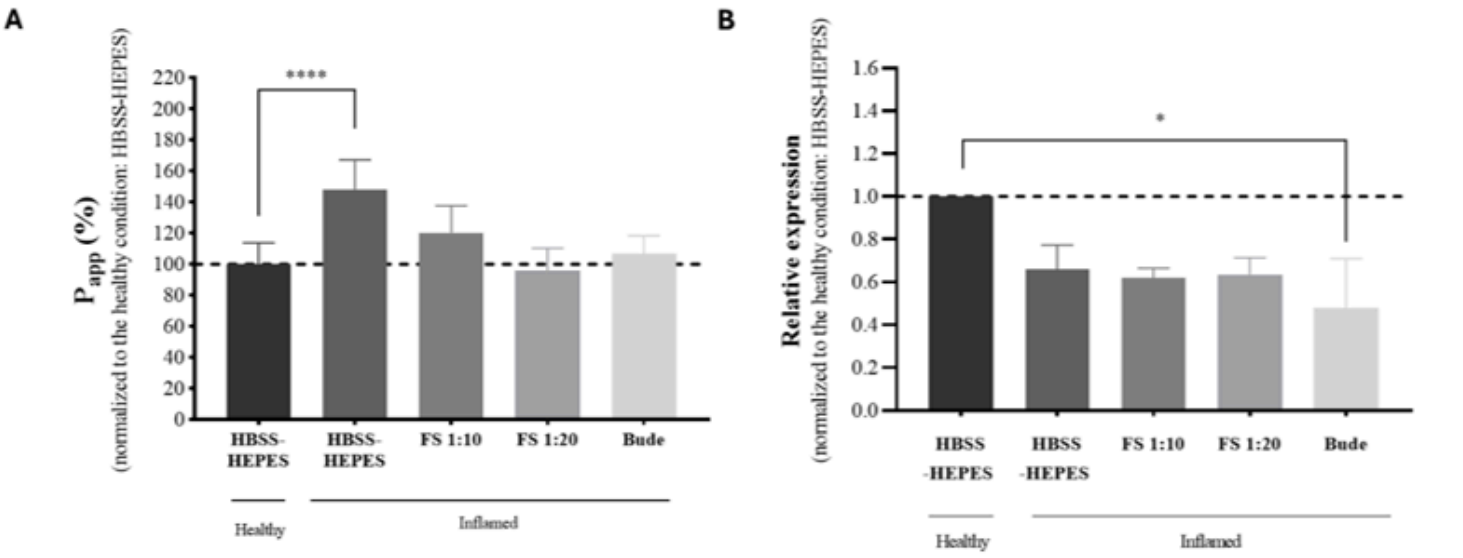


Figure 8

(A) Apparent permeability (P_{app}) of Lucifer Yellow, normalised to the healthy control condition (HBSS-HEPES). Caco-2/HT29-MTX (9:1) co-cultures were exposed to TNF-a (50 ng×mL-^{1}) in the culture medium for 48 h to induce barrier dysfunction, followed by 24 h incubation with HBSS-HEPES, fermentation supernatant diluted 1:10 or 1:20 in HBSS-HEPES, or budesonide (3 mM in HBSS-HEPES). Values are presented as mean ± SD; N = 3 independent experiments, with n = 4 technical replicates per experiment. **(B)** Relative occluding gene expression in differentiated Caco-2/HT29-MTX co-cultures exposed to HBSS-HEPES (healthy control) or TNF-a (50 ng×mL-^{1}) in the culture medium for 48 h, followed by 24 h incubation with HBSS-HEPES, fermentation supernatant diluted 1:10 or 1:20 in HBSS-HEPES, or budesonide (3 mM in HBSS-HEPES). Values are presented as mean ± SD; n ≥ 2. Statistical significance is indicated by * ($p < 0.05$) and **** ($p < 0.0001$).

Supplementary Files

This is a list of supplementary files associated with this preprint. Click to download.

- SupplementarymaterialSR.docx